

# First-principles studies on electronic structure and optical properties of anatase TiO<sub>2</sub> doped with Sn

MING HE<sup>1</sup>, YONGZHENG ZHU<sup>2,\*</sup>, SHUANG ZHENG<sup>2</sup>, SHUANG XING<sup>2</sup>, SHIMIN LIU<sup>2</sup>, BO SONG<sup>3</sup>

<sup>1</sup>*School of Physics and Materials Engineering, Dalian Minzu University, Dalian, 116600, PR China*

<sup>2</sup>*School of Science, Dalian Jiaotong University, Dalian, 116028, PR China*

<sup>3</sup>*Academy of Fundamental and Interdisciplinary Sciences, Harbin Institute of Technology, Harbin, 150080, PR China*

The relationship between electronic structure and some optical properties of Sn doped titanium dioxide (TiO<sub>2</sub>) was investigated by first principles calculation based on density function theory (DFT). The influence of dopant concentration or distance on the electronic structure and optical properties were studied. The gradual increase of Sn doping makes the absorption edge of TiO<sub>2</sub> red-shift and enhances the optical performance in the visible light region. Furthermore, experiments have detected that the bandgap of TiO<sub>2</sub> becomes bigger as the distance between two doped Sn atoms increases. The findings will provide certain theoretical basis for the present field of energy research.

(Received February 8, 2023; accepted February 12, 2024)

**Keywords:** Sn-doped TiO<sub>2</sub>, First-principles, Optical properties, Electronic structure

## 1. Introduction

As an important semiconductor, TiO<sub>2</sub> has many applications in hydrogen production, air purification and self-cleaning fields owing to its low cost, high chemical stability and less toxicity[1]. There mainly exist three basic crystalline phases for TiO<sub>2</sub> such as, rutile (*P4<sub>2</sub>/mmm*), brookite (*Pbca*), and anatase (*I4<sub>1</sub>/amd*)[2]. Among them, anatase TiO<sub>2</sub> has attracted particular attention for its more excellent photocatalytic activity and stability[3]. However, the wide bandgap (~3.2 eV) of anatase TiO<sub>2</sub> makes it can only be stimulated by ultraviolet (UV) light effectively, which significantly limits its working efficiency[4]. Therefore, tailoring the bandgap of TiO<sub>2</sub> is expected to be helpful to improve the photo-catalyst efficiency.

Jiang et al. pointed out that doping proper metal ions into TiO<sub>2</sub> can narrow the bandgap and reduce the electron-hole recombination rate to improve optical efficiency[5]. This method can introduce defects on the surface of semiconductors or change the lattice parameters of crystals[6, 7]. Li et al.[8] improved the optical properties of anatase TiO<sub>2</sub> systems by rare earth elements (La/Ce/Pr/Nd) doping. Vazquez et al.[9] proved that Sn<sup>4+</sup> doping increased the specific surface area of TiO<sub>2</sub> and improved the photocatalytic performance of TiO<sub>2</sub>. Jiang et al.[5] found Sn<sup>4+</sup> doping was effective in reducing the bandgap and could improve the photocatalytic activity of TiO<sub>2</sub> in the visible light region.

Due to the complex experimental conditions, diversified sample preparation routes and different

methods of optical response measurement, there are still many arguments on the effect of metal ion doping on the optical properties of TiO<sub>2</sub>[10, 11]. Compared with experiments, theoretical analysis may overcome the uncertainty of experimental factors and obtain a physical insight of the doping effects.

The first-principles calculation based on DFT is proven to be an effective method to reveal the electronic states of the doping system[12, 13]. Run et al.[14] found the amount of doped Sn ions plays a key role in the optical absorption spectrum, leading to red-shift or blue-shift of the edge. Bakhtawar et al.[15] drew a conclusion that mono-doped or co-doped TiO<sub>2</sub> by Ni and Eu substituting for Ti can reduce the bandgap of TiO<sub>2</sub>, which contributes to more visible light absorption. Khan M et al.[16] used Pr, N, and Ga as potential dopants, mono-, co-, and tri-doped models were established and achieved a better optical result.

However, there has been no detailed report on the structure and optical properties of Sn ions-doped TiO<sub>2</sub> from the perspective of microscopic information. In this work, using a combination of experiment and DFT calculation, we systematically investigated the structure and optical properties of Sn-doped anatase TiO<sub>2</sub>. The influence of Sn dopant's atomic separation and doping concentration on the band gap and optical properties of TiO<sub>2</sub> were studied.

## 2. Experimental and computational methods

Because of the similarity of ionic radii between Sn<sup>4+</sup>(0.690 Å) and Ti<sup>4+</sup>(0.605 Å), it is beneficial for Ti<sup>4+</sup>

to be replaced by Sn<sup>4+</sup> in the TiO<sub>2</sub> lattice to form a stable solid solution[17]. The synthesis of Sn doped TiO<sub>2</sub> were performed using a hydrothermal method. The titanium (IV) oxysulfate hydrate (TiOSO<sub>4</sub>) precursor was prepared in aqueous solution by dissolving 12.8 g (2.5 M) of TiOSO<sub>4</sub> in 32 ml of distilled water under constant stirring for 25 min to get a clear red solution ([Ti] = 0.4 M). Then Sn tin (IV) chloride (SnCl<sub>4</sub>) was added to TiOSO<sub>4</sub> solution at different weight ratios of Sn and Ti: 0.35%, 0.40% and 0.50%. The prepared solution was placed in a PTFE autoclave (volume 50 ml) and heated with a rate of 2.5°/min. During the synthesis the temperature was kept at 200 °C for 6 h with an accuracy of ±2 K. Then the prepared TiO<sub>2</sub> nanoparticles were washed six times in distilled water and two times in ethanol. The powder obtained by centrifugation was then dried in the oven. Finally, the dried nanoparticles were annealed in air at 500 °C for 30 min (heating rate is 5 °C/min). All the chemicals are of analytical grade and used without further purification. An ultraviolet-visible (UV-Vis) spectrophotometer was used to test the change of light absorption property. Based on the first-principles DFT [18] code, the plane-wave ultrasoft pseudopotential[19] (USP) calculation was used in the Cambridge Serial Total Energy Package (CASTEP) module[20, 21]. The electron exchange and related effects are handled by Perdew, Burke and Eruzerh (PBE) of Generalized Gradient Approximation (GGA).

Anatase TiO<sub>2</sub> has a tetragonal structure (space group: *I4<sub>1</sub>/amd*, lattice parameters:  $a=b=3.784$  Å,  $c=9.515$  Å,  $\alpha=\beta=\gamma=90^\circ$ )[22] and contains four Ti atoms and eight O atoms in the conventional cell. For geometry optimizations and the optical properties calculations for doped anatase TiO<sub>2</sub>, the *k*-points set 3×3×2 was used for the 48-atom 2×2×1 supercell. The wave functions of valence electrons were expanded using a plane-wave with an energy cut-off set to 340 eV in all calculations. The convergences were set as 2.0×10<sup>-5</sup> eV/atom for total energy, 0.05 eV/Å for maximum force[14], 0.1 GPa for maximum stress and 0.002 Å for maximum displacement of atoms convergence. The effects of Sn doping with different concentrations and atomic spacing on the bandgap and photo-activity of TiO<sub>2</sub> were simulated and discussed.

### 3. Results and discussions

Fig. 1 shows the 48-atom 2×2×1 supercell of anatase TiO<sub>2</sub>, and four typical positions of Ti were labeled by numbers 0, 1, 2 and 3. Sn atoms were used to replace certain Ti atoms. When doped with two Sn atoms, there were three species of doping atomic positions, named as Sn@(0,1), Sn@(0,2), and Sn@(0,3), respectively.

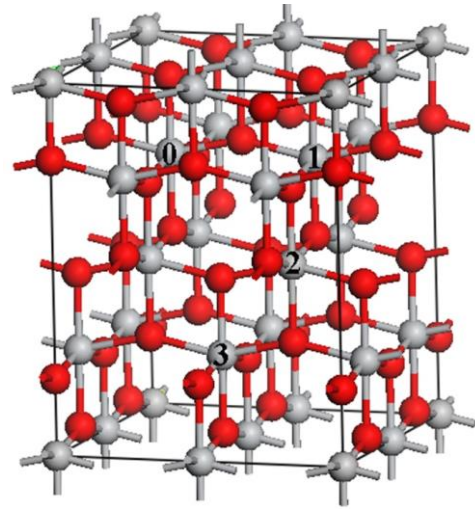


Fig. 1. The 48-atom 2×2×1 supercell of anatase TiO<sub>2</sub>; Ti<sub>14</sub>Sn<sub>2</sub>O<sub>32</sub>: Sn@(0,1), Sn@(0,2), Sn@(0,3) (color online)

The specific atomic distances between two doped Sn atoms were listed in Table 1. Fig. 2 shows four band structures of Ti<sub>16-x</sub>Sn<sub>x</sub>O<sub>32</sub> (x=0,1,2,3) with different doping concentration. The 0 eV energy level was set as Fermi level.

Table 1. The distance between two Sn atoms doped at (0,1), (0,2) and (0,3) positions

Ti <sub>14</sub> Sn <sub>2</sub> O <sub>32</sub>	Atom
(0,1)	3.807
(0,2)	4.900
(0,3)	5.557

The band structure of pure anatase TiO<sub>2</sub>(shown in Fig. 2(a)) exhibits an indirect band gap with a value 2.268 eV. This result obtained was below the experimental value of 3.2 eV[23], which was attributed to limitations of DFT[24]. However, the conduction band minimum (CBM) of Ti<sub>16-x</sub>Sn<sub>x</sub>O<sub>32</sub> (x=1,2,3) lie at the G point, and the valence band maximum (VBM) lie at G point approximately in the first Brillouin zone. So they are all can be seen as direct band gap semiconductors[25]. The energy levels of impurity were found to be introduced in the band gap via doping. There is an energy level locating at around 0.0168 eV, which is corresponding to the Sn atom substituting for Ti atom. The energy gap is plotted in Fig. 2(b) and calculated to be 2.207 eV. So, the impurity's states introduced at the VBM result in a narrower band gap compared with pure TiO<sub>2</sub>. In this series, the band structures of two heavier doped TiO<sub>2</sub> are presented in Fig. 2(c)-2(d), whose band gap energy are 2.138 eV and 2.117 eV, respectively. Significantly, after the increase of the Sn-doping concentration (about 6.25 to 18.75 at%), the narrower energy gaps were generated. It is consistent with Tm-doped anatase TiO<sub>2</sub>[26] and the results of Ning et al.

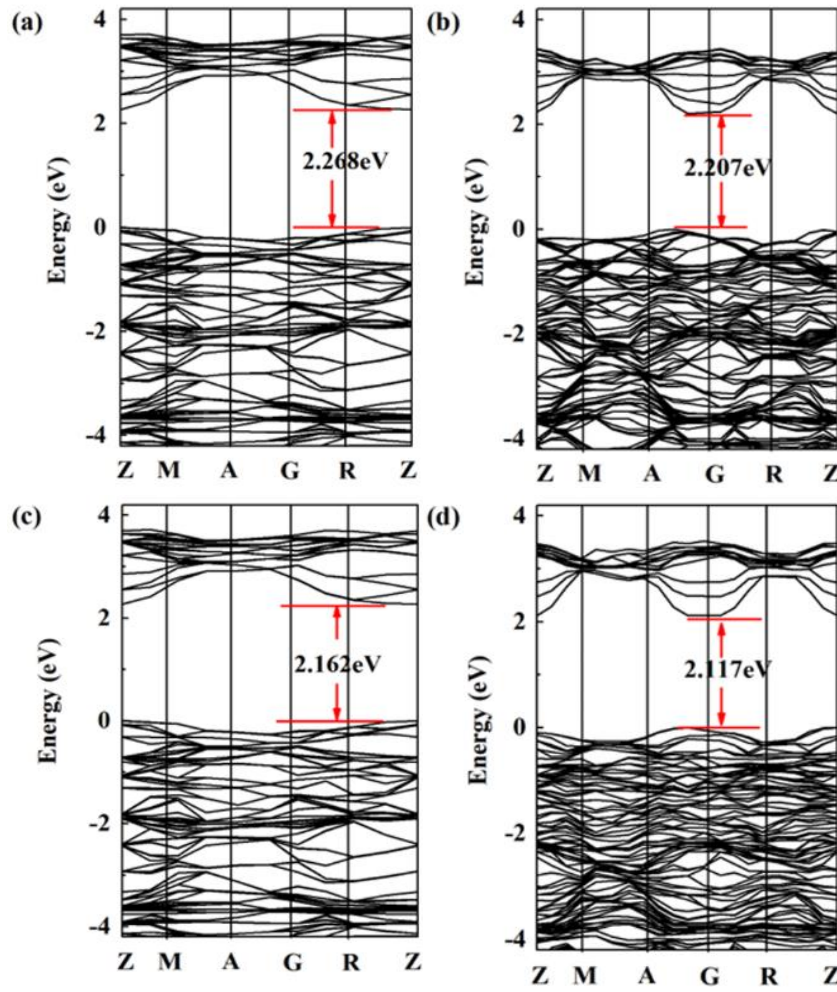


Fig. 2. Band structure of Sn-doped  $\text{TiO}_2$  with different concentrations: (a) pure; (b) 1/16; (c) 2/16; (d) 3/16 (color online)

This work also studies the effect of different dopant atomic distances on the energy bandgap and DOS. The band structures of the materials with three different Sn atom spacing are presented in Fig. 3. Likewise, the CBM and VBM all lie at G point in the Brillouin zone from Fig. 3(a)-(b). The bandgap of Sn@(0,1) is smallest

because the influence of the interaction between dopant particles becomes weaker[27] along with the increasing of the distance between atoms. As a result, the width of bandgap increases to 2.307 eV and 2.356 eV for Sn@(0,2) and Sn@(0,3), respectively. Meanwhile, the CB becomes wider as well.

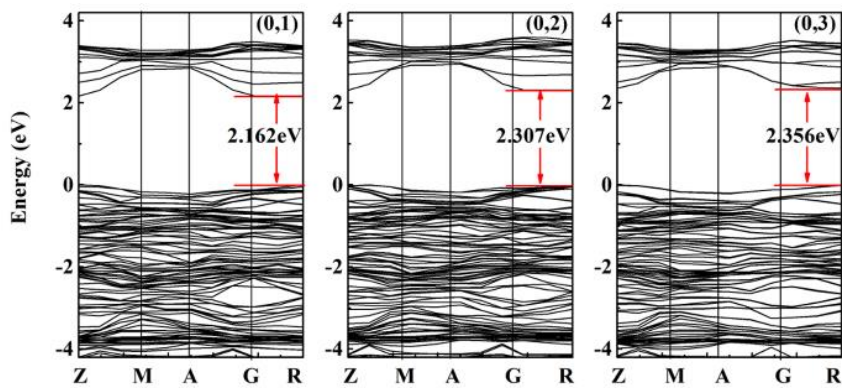


Fig. 3. Band structure of Sn-doped  $\text{TiO}_2$  with different dopant Sn separation: Sn@(0,1), Sn@(0,2), Sn@(0,3) (color online)

The total density of states (TDOS) and partial

density of states (PDOS) for undoped and Sn-doped

TiO<sub>2</sub> concentration of 6.25 at% are shown in Fig. 4. The Fermi level is represented by 0 eV energy. For pure anatase TiO<sub>2</sub> [Fig. 4(a)], in the conduction band (CB) from 0 to 10 eV is mainly composed of Ti-3d states. The lower valence band (VB) with energy in the range of -20 to -15 eV, is dominated by O-2s states. The upper VB from -10 eV to 0 eV is contributed mainly from O-2p and Ti-3d states. This indicates that the inter-band transitions of electrons were mainly determined by jumping from O-2p to Ti-3d states. As shown in Fig. 4(b), Sn doping introduces the Sn-5s and Sn-5p states in the VB near the Fermi level. The introduced hybridization of Sn-5p and O-2p states causes the VB to cross the Fermi surface and approach to CB, resulting in a narrower band gap. Many Sn-5s states are mixed with the Ti 3d states and located at the CBM. In this case, the inter-band transitions mainly involve the jumping from the Sn-5p to Ti-3d states.

As a consequence, the impurity bands introduced by

Sn doping can lead to the narrowing of the band gap and improve the solar photon absorptivity. Based on the TDOS of different doping concentration shown in Fig. 5, the incorporation of the Sn atom can modify the density of the states (DOS). The variations of both VB and CB characters take place with the increase of doping concentration. The VB maximum gradually shifts upward from the localization of 0.908 eV for pure TiO<sub>2</sub> to 0.922 eV for Ti<sub>15</sub>Sn<sub>1</sub>O<sub>32</sub>. Compared with pure TiO<sub>2</sub>, the valence bandwidth of Sn-doped TiO<sub>2</sub> also enlarges with the increase of the Sn concentration. However, the CB has a different trend from the VB analyzed above. In Sn doping case, the CBM moves down to a lower energy that contributes to the band gap narrowing.

Combining Fig. 4 and Fig. 5, it is found that the variation of band gap width with Sn doping concentration is mainly attributed to the Sn-5p states' movement[17].

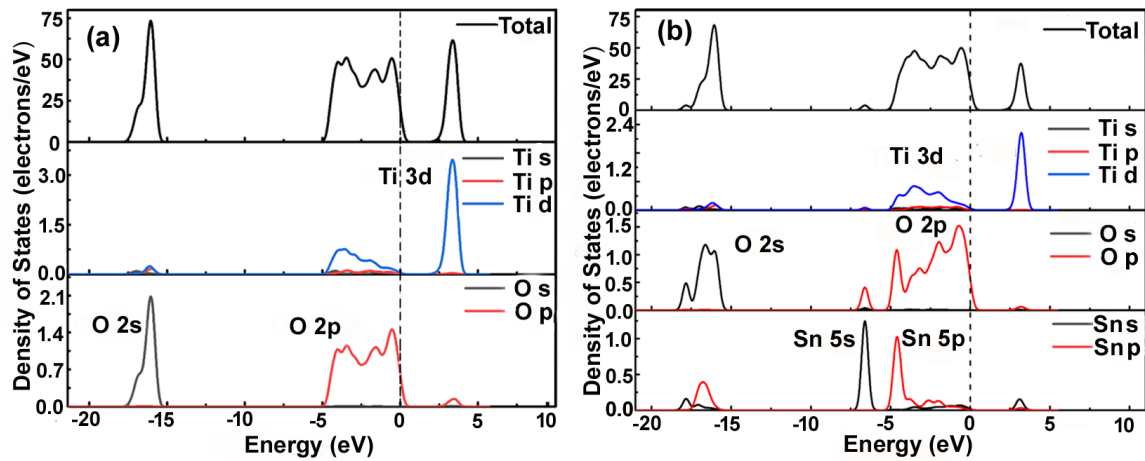


Fig. 4. The partial density of states of pure TiO<sub>2</sub> and 1/16 concentration Sn-doped TiO<sub>2</sub> (color online)

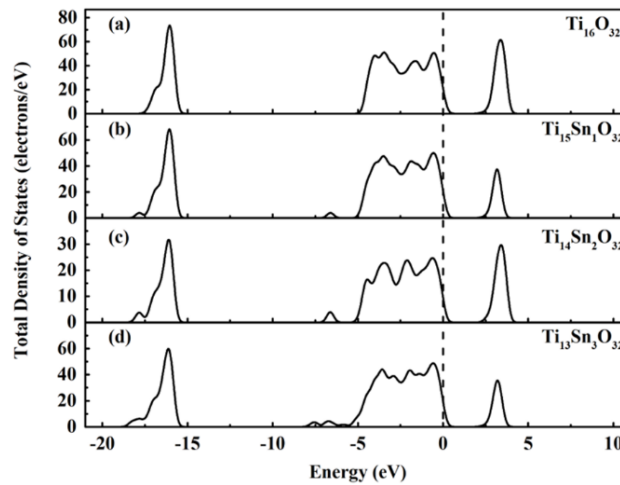


Fig. 5. The total density of states of pure TiO<sub>2</sub>, 1/16, 2/16, and 3/16 concentration

The optical property is of certain importance for TiO<sub>2</sub> in the application[28, 29]. Absorption coefficient, reflectivity, refractive index, dielectric function and

electrical conductivity usually highlight the significance of optical properties[30]. First, the TiO<sub>2</sub> light absorption spectrum was calculated and compared with the

experimental results, which was shown in Fig. 6. In Fig. 6(a), comparison of the calculated absorption spectra for  $\text{TiO}_2$  and  $\text{Ti}_{16-x}\text{Sn}_x\text{O}_2$  ( $x=0, 1, 2, 3$ ) was presented. The comparison results show that the light absorption edge shifts from the near-ultraviolet region (around 400 nm) to visible light (400-700 nm) along with the increase of Sn concentration. Fig. 6(b) gives the experimental absorption spectra of 0.35%, 0.40% and 0.50% concentration of Sn-doped  $\text{TiO}_2$ . The absorption coefficients calculated are consistent with the experimental ones and both decrease in the visible light region as shown in Fig. 6. The red-shift of visible-light absorption edge [27] is expected to result in a larger

visible light wavelength coverage[31] and the a better absorption of visible light. In addition, the other three optical properties of  $\text{TiO}_2$  and  $\text{Ti}_{16-x}\text{Sn}_x\text{O}_2$  ( $x=0, 1, 2, 3$ ) were calculated and results were shown in Fig. 7. Fig. 7(a)-(b) give the comparison of the reflection and refraction spectra of the four materials of different dopant concentration. At certain wavelength, the reflection and refraction decrease with the increasing of the dopant concentration.

This result agrees well with the increase in light absorption in Fig. 6. Fig. 7(c) and (d) shows the conductivity and dielectric functions in the low-energy region (0~10 eV), respectively.

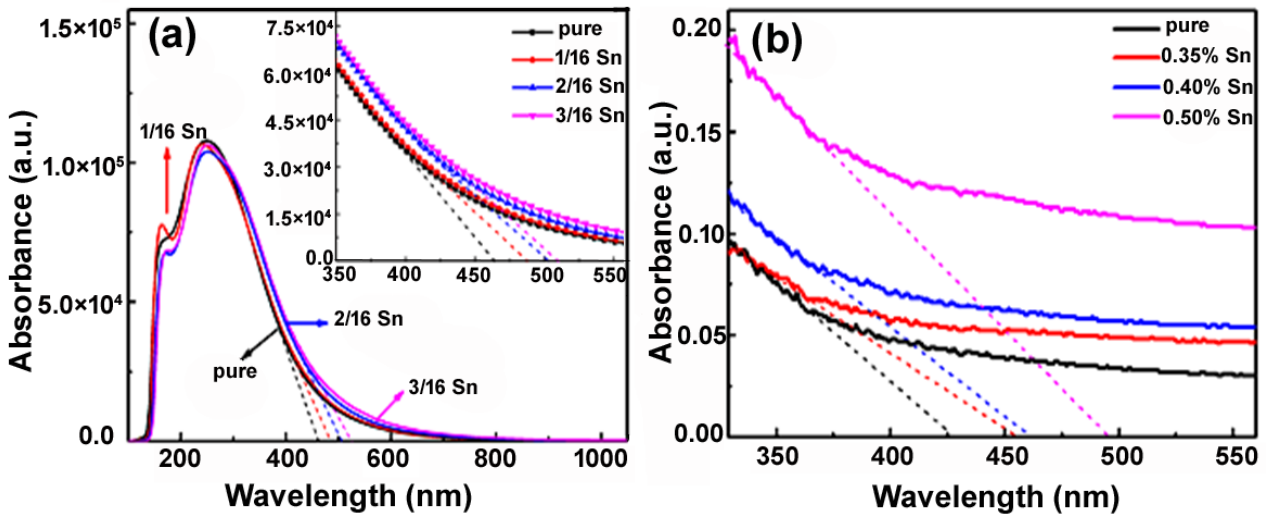


Fig. 6. Comparison of (a) calculated and (b) experimental light absorption rates between pure  $\text{TiO}_2$  and three concentrations of Sn-doped  $\text{TiO}_2$  (color online)

It can be seen that in the low-energy region, the intensity varies with the Sn concentration for certain energy. The strongest conductivity, reflection coefficient and dielectric functions occur at Sn concentration 2/16. The optical conductivity is given by:

$$\sigma = \sigma_1 + i\sigma_2 = -i \frac{\omega}{4\pi} (\varepsilon - 1) \quad (1)$$

It can be seen that the real part of conductivity and the imaginary part of  $\varepsilon$  present positive correlation. The reflection coefficient can be obtained as:

$$R = \left| \frac{\sqrt{\varepsilon_1 + i\varepsilon_2} - 1}{\sqrt{\varepsilon_1 + i\varepsilon_2} + 1} \right|^2 = \left| 1 - \frac{2}{\sqrt{\varepsilon_1 + i\varepsilon_2} + 1} \right|^2 \quad (2)$$

The reflection coefficient and the imaginary part of  $\varepsilon$  also present positive correlation. So, conductivity, reflection coefficient and dielectric functions have similar trends. This low energy peak can be identified according to the DOS mentioned above and linked with the electron transition from O-2p orbitals to Ti-3d or Sn-5p to Ti-3d orbitals. This low energy peak occurs because the increase in Sn concentration enhances the Sn-5p orbitals. So more electrons jump across the band gap and the resultant peaks become higher and stronger.

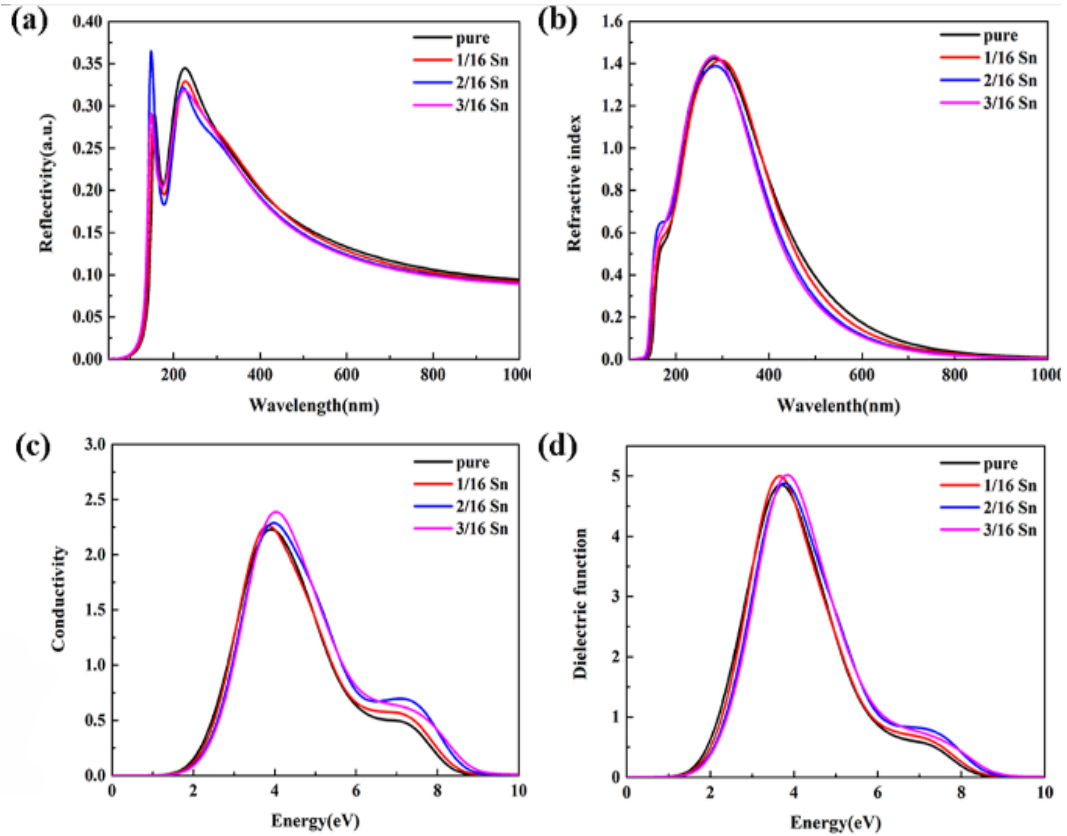


Fig. 7. Reflectance spectrum, refraction spectrum, electrical conductivity, and dielectric function of pure and Sn-doped TiO<sub>2</sub> of three concentrations (color online)

At the same time, the influence of different Sn atoms' spacing on TiO<sub>2</sub> electronic structure was studied. In the total DOS (shown in Fig. 8), the lower VB is almost unchanged, and the upper VB, as a part of the VBM moves to the left. The above DOS movement of

(0,3) configuration is most significant. The CB moves to the right, and the gap between them tends to expand. The result matches the information expressed by the band diagram and verifies each other.

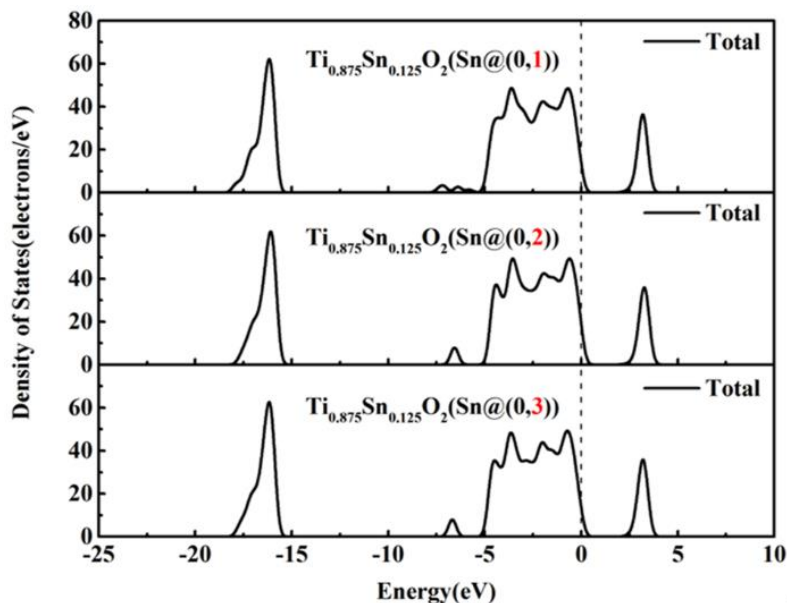


Fig. 8. Energy band and total density of states of two Sn atoms doped TiO<sub>2</sub> with different dopant atom distances (color online)

There have been a series of calculations to analyze optical properties for  $\text{TiO}_2$  doped with different Sn atomic distances, as seen in Fig. 9. Where (a) (b) (c) (d) are absorption spectrum, reflection spectrum, conductivity and dielectric function. As reported in Fig. 9(a), the absorption edge present blue-shift with the increase of atomic spacing, and the visible light

coverage area shrinks. Smaller atomic spacing can be realized by heavier doping and is expected to improve photocatalysis efficiency in the visible light region, but its absorption capacity becomes poor. On the contrary, as seen from the reflection spectrum of Fig. 9 (b) that the black line (0,1) has the worst reflection effect.

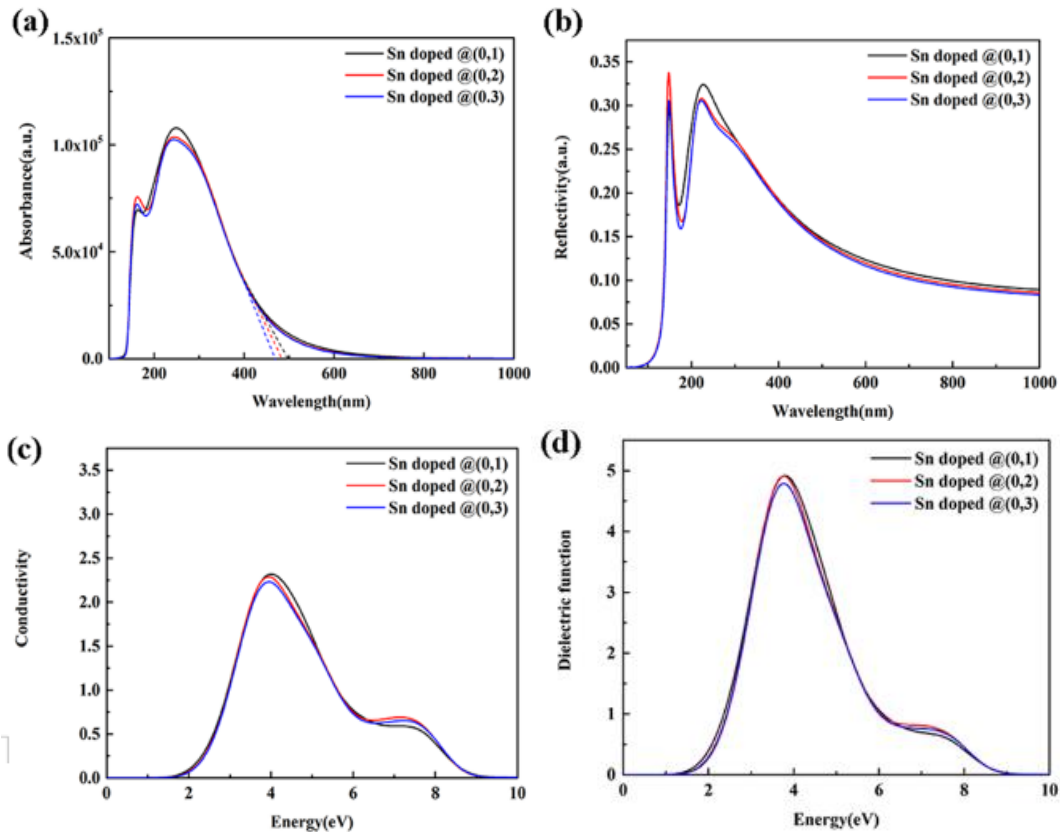


Fig. 9. Reflectance spectrum, refraction spectrum, electrical conductivity, and dielectric function of two Sn atoms doped  $\text{TiO}_2$  with different atom distances (color online)

It can be seen that the increase in the distance between atoms is not good for the absorption of visible light. Because most of the visible light is reflected, the photocatalytic efficiency is thought to be low. In contrast, the blue line (0,3) has the most potent reflection effect. As shown in Fig. 9(c) and (d), the electrical conductivity and dielectric parameters of the position (0,1) with the smallest interatomic distance are higher than that of (0,2) and (0,3), no matter in the low energy region of 0~10 eV or the high energy region of 33~38 eV.

#### 4. Conclusions

In conclusion, based on first-principles calculations and spectroscopic study, this work discusses the relationship between the electronic structure and optical properties of Sn doped  $\text{TiO}_2$ . Band structure and DOS character were studied under the situation of Ti ions

replacement with Sn in the forms of three concentrations or atomic distances. In terms of electronic structure, the energy band diagram present a direct bandgap semiconductor feature when  $\text{TiO}_2$  was doped with Sn atoms. The doping of Sn will introduce Sn 5s and 5p states, and their hybridization with the Ti 3d state of Ti atoms can occur. That will cause the VBM to move up and the forbidden bandwidth to become smaller. For optical properties, the introduction of Sn will make the absorption edge of  $\text{TiO}_2$  red-shift, and the effect becomes evident with the increase of doping amount. The introduction of Sn enhances the absorption of the material in the visible light region, while reduces the energy of reflection and refraction. The spacing of Sn atoms is related to the effect of inter-atomic interaction on photocatalysis. The strength of interaction between the particles reduces as the distance of two Sn atoms increases, which is not beneficial for the decrease in bandgap. The research results can provide certain

theoretical support for the research and application in the field of photocatalysis.

### Acknowledgements

This work was sponsored by the National Natural Science Foundation of China under Grant 52072058, 52171229 and U21A2074, Liaoning Revitalization Talents Program under Grant XLYC1807173, Liaoning BaiQianWan Talents Program (2021921012), Science and Technique Foundation of Dalian (2022JJ11CG003), Science and Technique Foundation of Liaoning Province (2023JH1/10400057, 2023JH1/10400080).

### References

- [1] R. Daghrir, P. Drogui, D. Robert, *Industrial and Engineering Chemistry Research* **52**, 3581 (2013).
- [2] Z. G. Mei, Y. Wang, S. Shang, Z. K. Liu, *Computational Materials Science* **83**, 114 (2014).
- [3] M. Khan, S. R. Gul, L. Jing, W. B. Cao, *Modern Physics Letters B* **29**, 1550022 (2015).
- [4] X. Liu, M. Khan, W. Liu, W. Xiang, M. Guan, P. Jiang, W. B. Cao, *Ceramics International* **41**, 3075 (2015).
- [5] H. B. Jiang, J. Xing, Z. P. Chen, F. Tian, Q. Cuan, X. Q. Gong, H. G. Yang, *Catalysis Today* **225**, 18 (2014).
- [6] Y. Fang, T. Xu, Y. Zhang, X. J. Kong, J. Liu, S. Cui, D. Wang, *Journal of Physics and Chemistry of Solids* **132**, 121 (2019).
- [7] D. Zhang, J. Chen, Q. Xiang, Y. Li, M. Liu, Y. Liao, *Inorganic Chemistry* **58**, 12511 (2019).
- [8] C. Li, Y. J. Zheng, S. N. Fu, H. W. Jiang, D. Wang, *Acta Physica Sinica* **65**, 037102 (2016).
- [9] I. Rangel-Vázquez, G. Del-Angel, V. Bertin, F. González, A. Vázquez-Zavala, A. Arrieta, J. M. Padilla, A. Barrera, E. Ramos-Ramirez, *Journal of Alloys and Compounds* **643**, S144 (2015)
- [10] Z. Gao, H. Yang, J. Mao, L. Kang, R. Zhang, S. Chai, J. Wu, W. Li, *Environmental Science and Pollution Research* **27**, 9748 (2020).
- [11] M. M. Khan, S. A. Ansari, D. Pradhan, M. O. Ansari, D. H. Han, J. Lee, M. H. Cho, *Journal of Materials Chemistry A* **2**, 637 (2014).
- [12] D. Li, R. Li, X. Qin, W. Yan, *Physics Letters A* **383**, 2679 (2019).
- [13] B. Liu, X. Zhao, *Applied Surface Science* **399**, 654 (2017).
- [14] R. Long, D. Ying, B. Huang, *Journal of Physical Chemistry C* **113**, 650 (2009).
- [15] B. Nazir, U. U. Rehman, S. Arshad, M. I. Arshad, N. Sabir, M. A. Javid, F. Iqbal, M. A. Nabi, *Materials Today: Proceedings*, (2020).
- [16] M. Khan, Y. Zeng, *Modern Physics Letters B* **34**, 2050388 (2020).
- [17] S. Mehraz, P. Kongsong, A. Taleb, N. Dokhane, L. Sikong, *Solar Energy Materials and Solar Cells* **189**, 254 (2019).
- [18] M. C. Payne, M. P. Teter, D. C. Allan, T. A. Arias, J. D. Joannopoulos, *Reviews of Modern Physics* **64**, 1045 (1992).
- [19] J. P. Perdew, K. Burke, M. Ernzerhof, *Physical Review Letters* **77**, 3865 (1998).
- [20] V. Milman, K. Refson, S. J. Clark, C. J. Pickard, J. R. Yates, S. P. Gao, P. J. Hasnip, M. I. J. Probert, S. Perlov, M. D. Segall, *J. Mol. Struct. (Theochem)* **954**, 22 (2010).
- [21] M. D. Segall, P. J. D. Lindan, M. J. Probert, C. J. Pickard, P. J. Hasnip, S. J. Clark, M. C. Payne, *J. Phys. Condens. Matter* **14**, 2717 (2002).
- [22] A. L. Linsebigler, G. Lu, J. T. Yates, *Chemical Reviews* **95**, 735 (1995).
- [23] G. Shao, Q. Deng, L. Wan, M. Guo, X. Xia, Y. Gao, *Journal of Nanoscience and Nanotechnology* **10**, 7092 (2010).
- [24] J. P. Perdew, M. Levy, *Physical Review Letters* **51**, 1884 (1983).
- [25] P. D. Sreedevi, R. Vidya, P. Ravindran, *Solar Energy* **190**, 350 (2019).
- [26] Z. N. Wei, C. L. Jia, *Optical Engineering* **54**, 037107 (2015).
- [27] R. H. Zhang, Q. Wang, Q. Li, J. Dai, D. Huang, *Physica B: Condensed Matter* **406**, 3417 (2011).
- [28] M. Mitronika, J. Profili, A. Goulet, L. Stafford, A. Granier, M. Richard-plouet, *Thin Solid Films* **709**, 138212 (2020).
- [29] P. S. Jadhav, T. Jadhav, M. Bhosale, C. H. Jadhav, V. C. Pawar, *Materials today: proceedings* **43**, 2763 (2021).
- [30] L. Kean, M. A. Mohamed, A. K. Mondal, M. F. M. Taib, M. H. Samat, D. D. Berhanuddin, P. S. Menon, R. Bahru, *Micromachines* **12**, 348 (2021).
- [31] X. Jiang, C. Li, S. Liu, F. Zhang, F. You, C. Yao, *RSC Advances* **7**, 24598 (2017).

\*Corresponding author: zhuyz1978@163.com